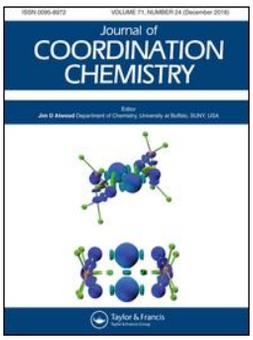

Taylor & Francis
Taylor & Francis Group

Journal of Coordination Chemistry

ISSN: 0095-8972 (Print) 1029-0389 (Online) Journal homepage: https://www.tandfonline.com/loi/gcoo20

Synthesis, crystal structure, spectral and electrochemical characterization, DNA binding and free radical scavenging studies of ferrocene-based thioureas

Bhajan Lal, Ammarah Kanwal, Ataf Ali Altaf, Amin Badshah, Faiza Asghar, Sadia Akhter, Shafiqullah Marwat, Syed Ishtiaq Khan & Muhammad Nawaz Tahir

To cite this article: Bhajan Lal, Ammarah Kanwal, Ataf Ali Altaf, Amin Badshah, Faiza Asghar, Sadia Akhter, Shafiqullah Marwat, Syed Ishtiaq Khan & Muhammad Nawaz Tahir (2019): Synthesis, crystal structure, spectral and electrochemical characterization, DNA binding and free radical scavenging studies of ferrocene-based thioureas, Journal of Coordination Chemistry, DOI: 10.1080/00958972.2019.1651846

To link to this article: https://doi.org/10.1080/00958972.2019.1651846

JOURNAL OF COORDINATION CHEMISTRY
https://doi.org/10.1080/00958972.2019.1651846

Synthesis, crystal structure, spectral and electrochemical characterization, DNA binding and free radical scavenging studies of ferrocene-based thioureas

Bhajan Lal[a], Ammarah Kanwal[b], Ataf Ali Altaf[c], Amin Badshah[d], Faiza Asghar[e], Sadia Akhter[c], Shafiqullah Marwat[c], Syed Ishtiaq Khan[c] and Muhammad Nawaz Tahir[f]

[a]Institute of Chemistry, Shah Abdul Latif University, Khairpur, Pakistan; [b]Cast Metals and Foundry Technology Centre (CM and FT) PCSIR, Daska, District Sialkot, Pakistan; [c]Department of Chemistry, University of Gujrat, Hafiz Hayat Campus, Gujrat, Pakistan; [d]Department of Chemistry, Quaid-i-Azam University, Islamabad, Pakistan; [e]Department of Chemistry, University of Wah, Wah, Pakistan; [f]Department of Physics, University of Sargodha, Sargodha, Pakistan

ABSTRACT

Thioureas are important building blocks in medicinal chemistry; ferrocenes as highly hydrophobic moieties induce very interesting qualities in medicinal compounds. In this article, we have synthesized four ferrocene incorporated N,N′-disubstituted benzoyl thioureas (**3a–3d**) with general formula C_5H_5-Fe-$C_5H_4C_6H_4$Cl-NH-CS-NH-CO-C_6H_4(H/CH_3). Molecular structures of these compounds were characterized in solid and solution phases. In solution molecular structures were established by ^{1}H and ^{13}C NMR and cyclic voltammetry. In the solid state their structures were characterized by elemental analyses and FTIR spectroscopy. Two of the compounds (**3a** and **3d**) had also been structurally determined by single crystal X-ray diffraction analysis. The electrochemical characterization showed a reversible process with one electron transfer from Fe(II) to Fe(III). The single crystal analysis showed strong intermolecular non-covalent interactions in these compounds. Molecular structures of these compounds were also studied by density functional theory (DFT) calculation . DFT studies showed good correlation between calculated parameters and experimental results of solution phase and solid state characterizations. Compounds **3a–3d** were evaluated for DNA interaction and antioxidant activity. These compounds interact with DNA via electrostatic forces and liberate significant binding constants and energies. Antioxidant potential –CSN***H*** and –CON***H*** groups induce same level of free radical scavenging ability in these compounds.

ARTICLE HISTORY
Received 22 February 2019
Accepted 19 July 2019

KEYWORDS
Ferrocene-based thioureas; crystal structure; redox nature; DFT calculations; DNA binding; free radical scavenging

CONTACT Amin Badshah aminbadshah@yahoo.com; Ataf Ali Altaf atafali_altaf@yahoo.com

Supplemental data for this article is available online at https://doi.org/10.1080/00958972.2019.1651846.

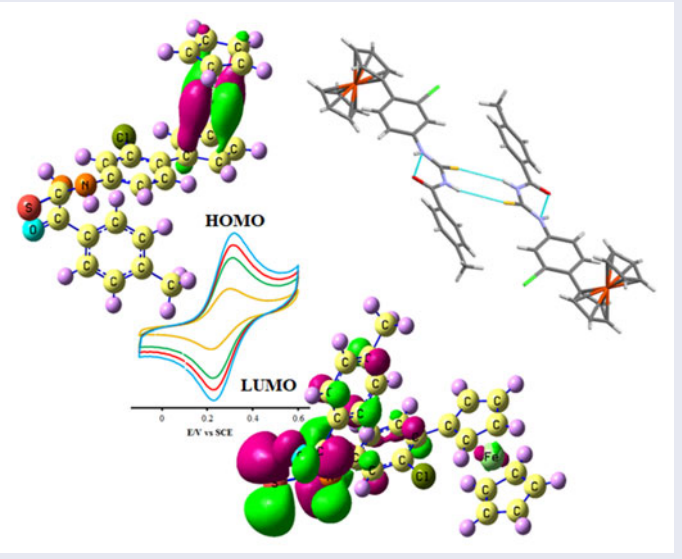

1. Introduction

For more than 50% of the treatments in the clinic to kill cancerous cells, platinum-based drugs like cisplatin, carboplatin and oxaliplatin are used [1]. Despite their tremendous success, their use has also been limited due to inherent and acquired resistance and the presence of a number of dose-limiting side effects [2]. The cytotoxicity of Pt-based anticancer drugs is related to their interaction with deoxyribosenucleic acid (DNA) that ultimately inhibits the transcription and replication resulting in cell death [3]. As a consequence of its particular chemical structure, cisplatin offers little possibility for rational improvements to increase its tumor specificity and thereby reduce undesired side effects. Organometallic compounds have recently been found to be promising anticancer drug candidates [4]. Organometallic compounds have great structural variety, far more diverse stereochemistry than organic compounds (for an octahedral complex with six different ligands, 30 stereoisomers exist), and by rational ligand design, provide control over key kinetic properties (such as hydrolysis rate of ligands) [5]. Furthermore, they are kinetically stable, usually uncharged, and lipophilic and their metal is in a low oxidation state [6]. Typical classes of organometallic complexes such as metallocenes, half-sandwich, carbene-, CO-, or π-ligands, which have been widely used for catalysis or bio-sensing purposes, have now also found application in medicinal chemistry [7]. Among metallocenes, ferrocene and its derivatives have been studied as potential chemotherapeutics [8, 9]. Thioureas are an important class of medicinal compounds [10–14]. Incorporation of ferrocenyl moiety in the structure of tamoxifen resulted in increased anticancer activity [15]. The anticancer activity of ferrocene derivatives is dependent on the oxidation state of iron in the ferrocene moiety with some results, indicating that the Fe(II) ferrocenyl compound is more active than Fe(III) ones [16]. Electron transfer reactions involving ferrocenium ion may generate reactive oxygen species (ROS) such as hydroxyl

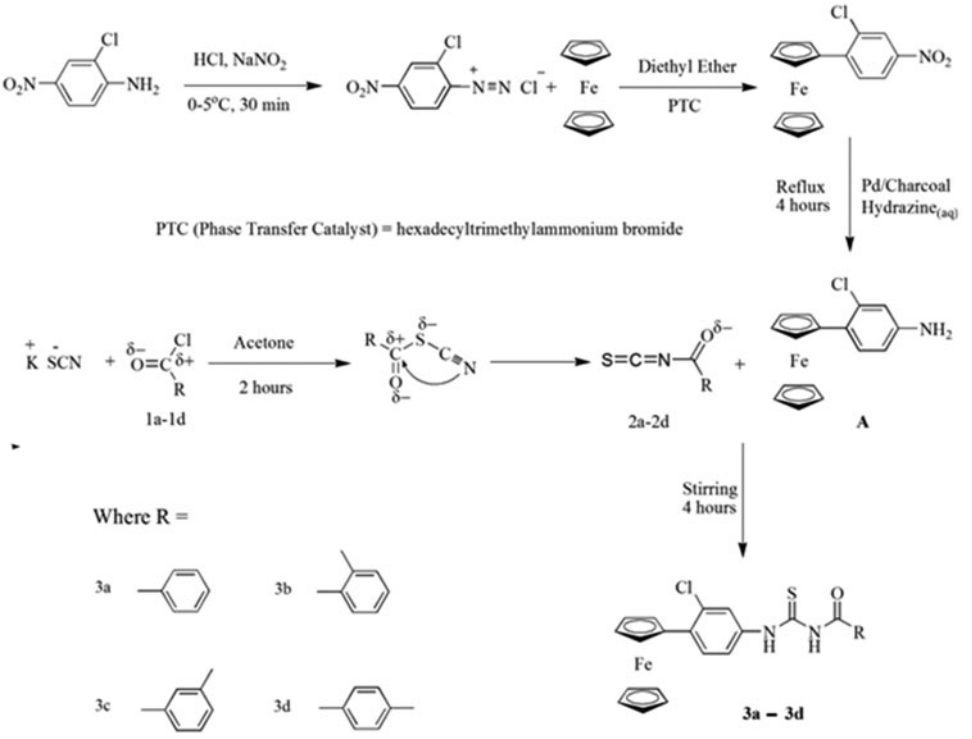

Scheme 1. The reaction scheme for synthesis of ferrocene incorporated N,N′-disubstituted thioureas.

radicals (•OH). ROS can cause damage to DNA [17] and may also be responsible for anticancer activity through the formation of radical metabolites that bring about biological damage in cancer cells [18]. Some ferrocene-based thioureas bearing significant activity have been published [19–22]. Herein we present the systematic synthesis, structural characterization, redox behavior, extent of DNA binding and free radical scavenging potency of some new ferrocene incorporated benzoylthioureas.

2. Results and discussion

2.1. Synthesis

The pathway adopted for synthesis of six new ferrocene incorporated N,N′-disubstituted thioureas is sketched in Scheme 1. Compounds **3a–3d** are synthesized by reacting 4-ferrocenyl-3-chloroaniline with freshly prepared isothiocyanates under N_2 in dry acetone [13, 19]. The compounds were structurally characterized by using different analytical techniques.

2.2. Solution phase characterization

In the solution phase, all products were characterized by ^{1}H and ^{13}C NMR, and electrochemical characterizations were made by cyclic voltammetry.

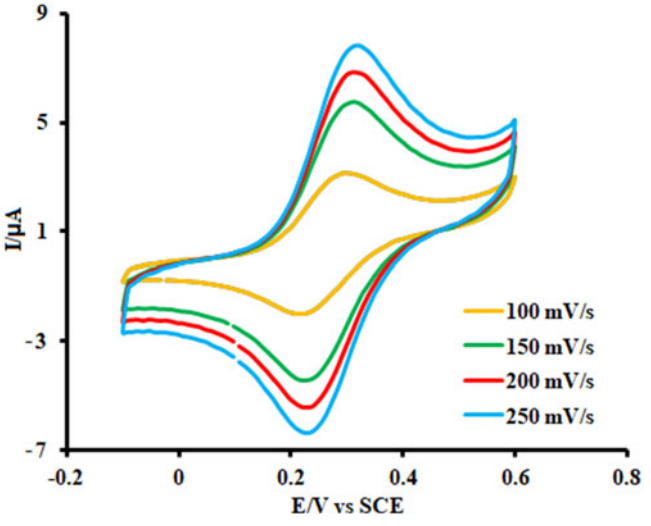

Figure 1. Cyclic voltammograms of 2 mM DMSO solution of **3d** (representative compound) at different scan rates (50–250 mV/s), obtained on a three electrode system: platinum disc working electrode, secondary calomel as reference electrode and platinum wire counter electrode.

The ^{1}H and ^{13}C NMR spectra of **3a–3d** were taken in DMSO as reported in Section 4. The ^{1}H NMR data showed that unsubstituted Cp-ring of ferrocene displayed singlet for five protons at 4.22–4.17 ppm; however, the substituted Cp-ring of ferrocene split into two signals in the region of 4.84–4.38 ppm. The methyl protons (attached to phenyl ring for **3b–3d**) are at 2.58–1.28 ppm as singlets with integral value of three. The substituted aromatic ring gave signals at 7.91–7.56 ppm [19–22]. The –CSN***H*** and –CON***H*** protons are downfield at 12.74–8.84 ppm. The multiplicity and intensity of signals were used to identify nonequivalent protons. The integration curve revealed that protons present in the molecule and the area under the curve were in agreement.

The ^{13}C NMR spectral data of **3a–3d** revealed that unsubstituted Cp-ring of ferrocene showed a singlet for five carbons at 69.86–69.73 ppm whereas the substituted Cp-ring of ferrocene split into three signals, the ipso carbon (attached to phenyl ring) at 83.68–83.49 ppm. The other two signals were at 68.87–67.94 ppm. The methyl carbon (attached to phenyl ring for **3b–3d**) is at 21.79–20.23 ppm. Compounds **3a–3d** exhibited signals for aromatic carbons at 145.10–121.80 ppm. The two most downfield signals are attributed to carbon of thiocarbonyl and carbonyl as weak signals at 178.01–166.92 ppm and 169.57–153.55 ppm, respectively [19–22]. The ^{1}H and ^{13}C NMR data for **3a–3d** are in agreement with the data for other similar compounds [19–22].

The cyclic voltammograms of **3a–3d** were scanned using a three electrode system in DMSO. Platinum disc working electrode, with surface area 0.071 cm^2, was used along with a secondary calomel reference electrode and platinum wire was kept as counter electrode. In cyclic voltammograms of **3d** (Figure 1) obtained at 100 mV/s scan rate, two signals were observed, one in forward scan at anodic potential (E_{pa}) of 285 mV with anodic peak current (I_{pa}) of 2.6 μA and the other one in reverse scan at cathodic potential (E_{pc}) 223 mV with cathodic peak current (I_{pc}) of −2.4 μA. The change

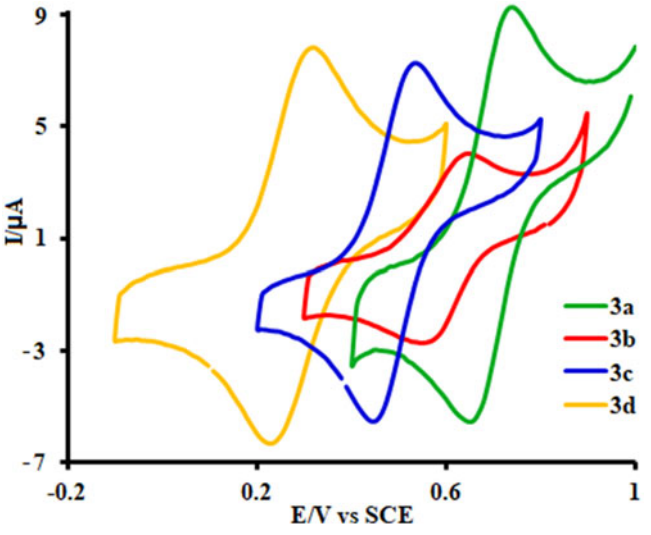

Figure 2. Cyclic voltammograms of 2 mM DMSO solution of **3a**, **3c** and **3d** at 250 mV/s scan rates (voltammogram for **3b** was recorded on 100 mV/s).

of scan rate on the voltammogram was studied by stepwise increments of 50 mV up to the scan rate 250 mV/s (Figure 1). No significant change was observed in the anodic/cathodic peak position by the variation of scan rate; increase in the magnitude of current was observed upon increasing the scan rate, indicating the reversibility of the electrochemical redox process [23]. The reversibility of the process was further confirmed from magnitude of the ratio of cathodic to anodic peak current ($I_{pc}/I_{pa} = 0.92 \approx 1$) that is almost equal to one [24]. The potential difference (ΔE_p) between the two peak potentials was $\Delta E_p = E_{pc} - E_{pa} = 62$ mV. This indicates that the number of electrons involved in the electrochemical process is $58/62 = 0.93 \approx 1$ [25]. Hence, these observations confirmed that the electrochemical reaction on the surface of platinum disc working electrode is a one electron reversible redox process [25]. Different ferrocene compounds give E_{pa} and E_{pc} values of 200–820 mV and 140–780 mV, respectively, for reversible redox of ferrocene (Fc) to ferrocenium (Fc^+) [20, 22, 26–28]. Therefore, the electrochemical reaction can be associated with the reversible redox process of Fc to Fc^+ and Fc^+ to Fc transformations in **3d** on the surface of working electrode.

Compounds **3a–3c** behave in a similar manner but are not discussed here. Figure 2 presents the voltammograms for these compounds. The diffusion of **3a–3d** on the surface of the electrode was calculated in terms of diffusion coefficient (D_o) by using Randles-Sevcik Equation (1) [25],

$$I_{pa} = 2.69 \times 10^5 n^{3/2} A C_o^* D_o^{1/2} \upsilon^{1/2} \quad (1)$$

where I_{pa} is the anodic peak current in ampere, υ is the scan rate in V s^{-1}, C_o^* is the concentration in mol cm^{-3}, A is the cross-sectional area of electrode in cm^2, n is the number of electrons involved in the reaction and D_o is the diffusion coefficient in $cm^2 s^{-1}$. The data obtained are reported in Table 1 and the experimental data are provided in the Supplementary Material.

Table 1. The electrochemical data (experimental electrode potentials compared with calculated energies of HOMO and LUMO levels), diffusion coefficient (D_o) of free compound, compound-DNA adduct, binding constant and binding energy of **3a**, **3b**, **3c** and **3d**.

Compound	E_{pa}, E_{pc} (mV)	E_{HOMO} (eV)	E_{LUMO} (eV)	D_o of free compound (cm^2s^{-1})	D_o of compound-DNA adduct (cm^2s^{-1})	Binding constant (M^{-1})	Binding energy (kJ mol^{-1})
3a	718, 652	−5.2455	−2.0637	1.7×10^{-7}	2.9×10^{-8}	3.1×10^{3}	19.92
3b	642, 578	−5.2461	−1.9579	2.0×10^{-7}	3.6×10^{-8}	2.4×10^{3}	19.28
3c	518, 453	−5.2300	−2.0109	2.0×10^{-7}	6.8×10^{-7}	2.8×10^{3}	19.66
3d	285, 223	−5.2268	−1.9886	2.4×10^{-7}	8.8×10^{-8}	4.1×10^{3}	20.61

2.3. In-silico characterization by density functional theory (DFT)

Computational calculations were undertaken for these electro-active compounds in order to complement the experimental results of cyclic voltammetry. The oxidation-reduction potentials of the synthesized ferrocenyl thioureas measured from cyclic voltammetry indicated parallel trend to that anticipated from the density functional theory (DFT) work.

The ease of reduction of the complexes varies as **3a** > **3b** >**3c** > **3d**. An analogous trend was attained from the E_{LUMO} values, i.e. the highest reduction potential and most negative E_{LUMO} value of **3a** correspond to easiest reduction [29–31]. A more negative E_{LUMO} favors addition of electrons as the energies of the orbitals are lowered. Figures 3 and 4 display the representative graphical demonstration of the HOMO and LUMO orbitals of **3a** and **3d**, respectively. The HOMO orbitals are localized on the ferrocene moiety (Fe metal), whereas the LUMO orbitals are extended over the thiourea functionality (containing electron-withdrawing N and O) and the terminal phenyl ring. The HOMO-LUMO energy gaps were in close agreement with the electrochemical band gaps computed from the difference between the oxidation and reduction potential of the species (Table 1) [32]. The E_{HOMO} values acquired from DFT were compared with the oxidation potentials achieved from the electrochemical measurements. The oxidation potentials observed experimentally for **3a–3d** fluctuate as **3d** >**3c** > **3b** > **3a**. This observation is supported from the DFT study by comparing the E_{HOMO} values, which are less negative for **3d**, signifying its ease of oxidation as compared to other compounds (Table 1).

DFT measurements also established the Mulliken charges on these molecular structures to determine the sites which are susceptible to electrophilic or nucleophilic attack (Figure 5) [33]. The explored molecules **3a–3d** have numerous probable sites for electrophilic (denoted by red color) and nucleophilic attack (symbolized by green color), as depicted in Figure 5(b,d) for **3a** and **3d**, respectively.

2.4. Solid phase characterization

In the solid state, the products were characterized by Fourier Transformation Infrared (FTIR) spectroscopy, and **3a** and **3d** were also characterized by single crystal X-ray diffraction.

The FTIR data are reported in Section 4. The data indicate that highest energy vibrations for these compounds (thiourea's N–H stretching bands) were observed at 3247–3422 cm^{-1} [12, 31]. A sharp signal at 1661–1673 cm^{-1} was observed for amide

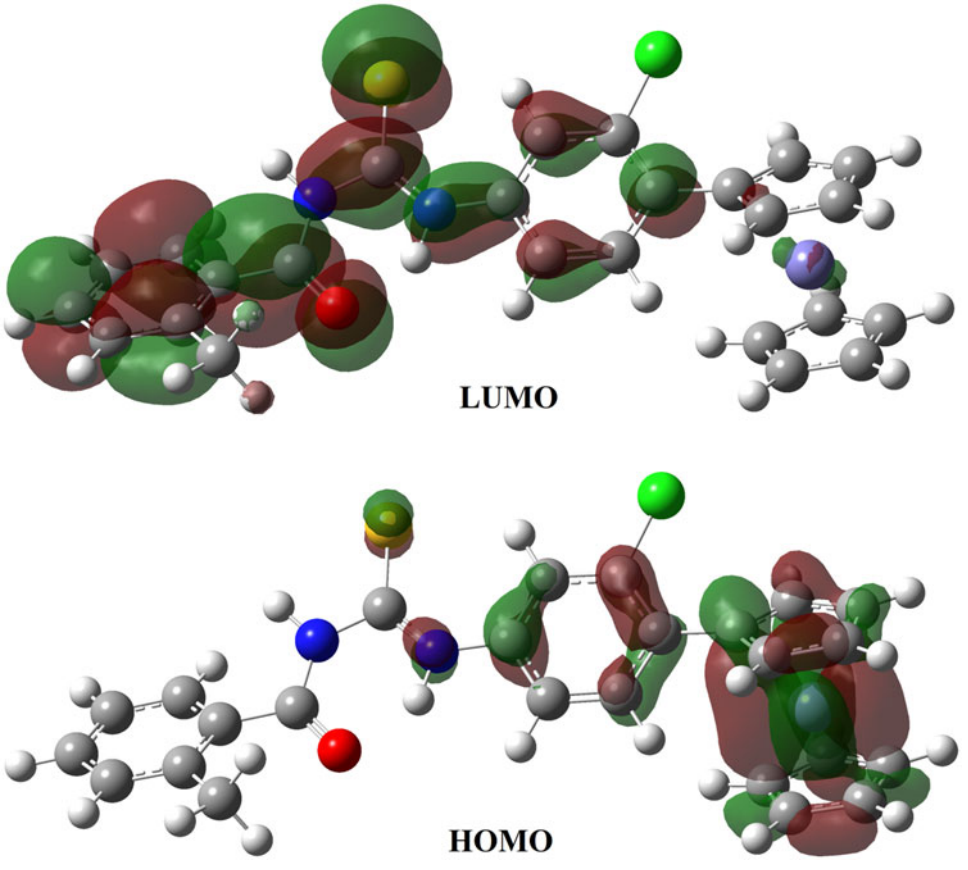

Figure 3. Graphical demonstration of HOMO and LUMO energy levels of **3b**.

based C = O, in agreement with literature data [34–36]. A broad signal for **3a–3d** was observed from 1036 to 1275 cm^{-1} that originated from the thiourea C = S [37]. However, the characteristic peak of the Fe-Cp stretching band appeared at 479–486 cm^{-1} [35, 36] and other C = C and C-H (sp^3 and sp^2) bands were observed in their usual regions [38].

2.5. Single crystal X-ray studies

Careful crystallization of **3a** and **3d** in toluene by slow evaporation yielded orange crystals suitable for single crystal X-ray diffraction analysis. Data pertaining to the data collection and structure refinement show that **3a** crystallized in the triclinic crystal system with $P\bar{1}$ space group. A multi-scan absorption correction method was used. The other crystal parameters calculated at 296 K using Mo K_α ($\lambda = 0.71073$) radiation were empirical formula $C_{24}H_{19}FeN_2OSCl$, unit cell dimensions $a = 7.6045(18)$ Å, $b = 11.712(3)$ Å, $c = 11.841(3)$ Å, $\alpha = 86.297(8)^\circ$, $\beta = 86.760(8)^\circ$, $\gamma = 81.079(9)^\circ$, $M = 474.77$, volume = 1038.5(4) $Å^3$, $Z = 2$, Density = 1.518 g/cm^3, $F(000)$ = 588.0, Crystal size = $0.27 \times 0.16 \times 0.14\ mm^3$, index ranges $(h, k, l)_{max}$ = (9, 14, 14), $(h, k, l)_{min}$ = (−9, −14,

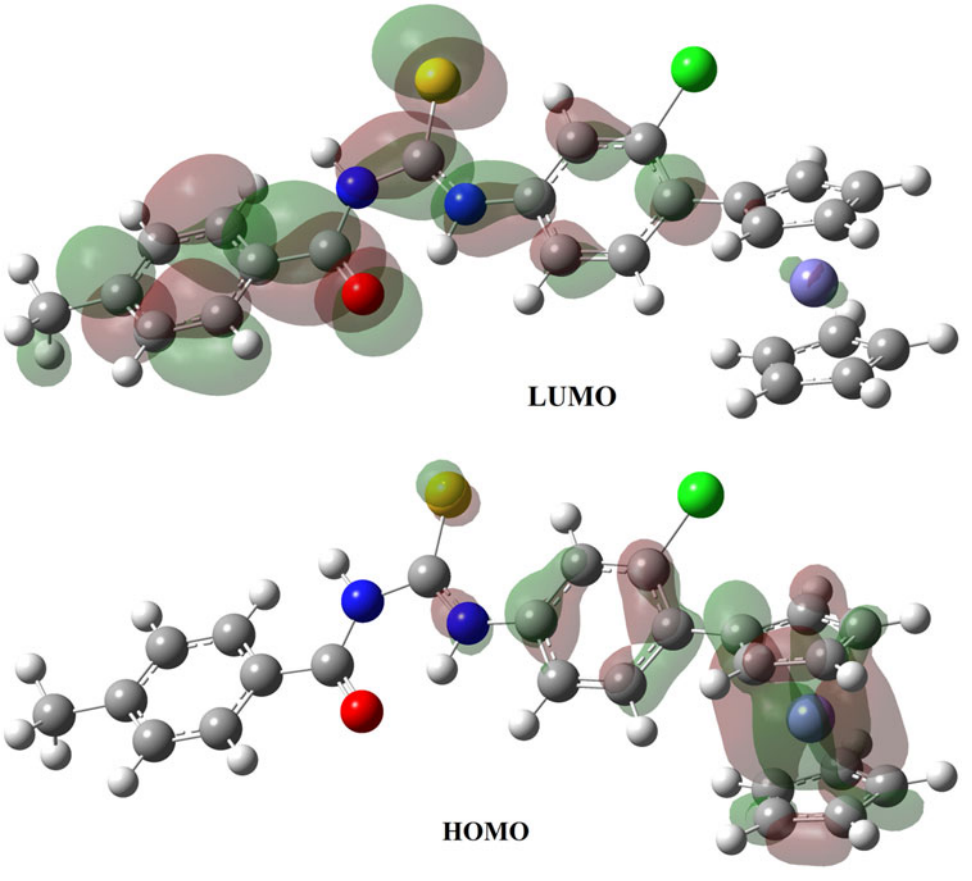

Figure 4. Graphical demonstration of HOMO and LUMO energy levels of **3d**.

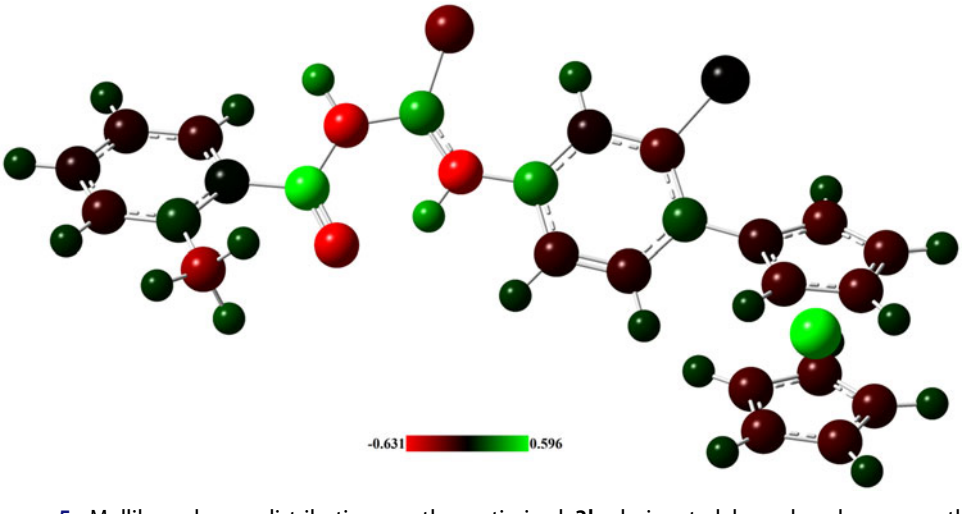

Figure 5. Mulliken charge distribution on the optimized **3b** designated by color change on the atoms with color scheme and scale (red for negative charge and green for positive charge). The numerical values of Mulliken charges for this molecule and all the other molecules calculated by DFT can be seen in the electronic supplementary data (Table S1).

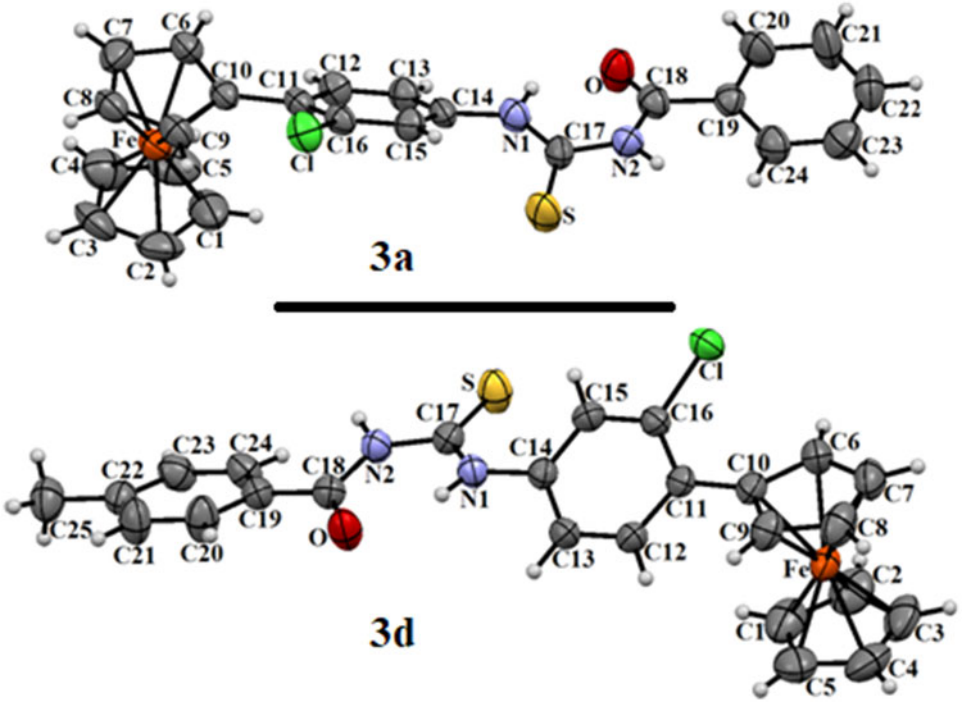

Figure 6. Molecular structures (50% probability ORTEP) of **3a** and **3d** with numbering schemes.

−14), total reflections = 4087, Mu = 0.974 mm^{-1}, θ_{max} = 26.00°, S = 0.995, R = 0.0662 and wR2 = 0.1843.

Compound **3d** crystallized in the triclinic crystal system with $P\bar{1}$ space group. A multi-scan absorption correction method was used. The other crystal parameters calculated at 296 K using Mo K_α (λ = 0.71073) radiation were empirical formula $C_{25}H_{21}FeN_2OSCl$, unit cell dimensions a = 7.7009(4) Å, b = 11.7399(6) Å, c = 11.9509(6) Å, α = 89.752(3)°, β = 88.039(2)°, γ = 86.517(3)°, M = 488.80, volume = 1077.83(10) Å^3, Z = 2, density = 1.506 g/cm^3, F(000) = 504.0, crystal size = 0.32 × 0.25 × 0.23 mm^3, index ranges (h, k, l)$_{max}$ = (9, 14, 14), (h, k, l)$_{min}$ = (−9, −14, −14), total reflections = 4250, Mu = 0.941 mm^{-1}, θ_{max} = 26.00°, S = 1.027, R = 0.0510 and wR2 = 0.0859.

Interatomic distances, bond angles and torsion angles can be seen in the crystallographic information files provided as supplementary material of the article. Figure 6 represents the molecular structures with numbering scheme for **3a** and **3d**. The intramolecular hydrogen bonding and intermolecular interactions present in these compounds are summarized in Table 2 and Figure 7.

The rings A (C6-C10), B (C11-C16), C (H_{N1}, N1, C17, N2, C18, O) and D (C19-C24) in **3a** and **3d** are planar. In **3a**, the root mean square (r.m.s) deviations of the rings A–D from planarity are 0.0008, 0.0077, 0.0448 and 0.0044 Å, respectively; in **3d** the r.m.s deviations of the rings A–D from planarity are 0.0019, 0.0091, 0.0535 and 0.0083 Å, respectively. Intramolecular hydrogen bonding in these structures exists as mentioned in Figure 7 and Table 2. This intramolecular hydrogen bonding (NH—O type) is responsible for the planarity of six atoms forming ring C in both compounds. This intramolecular hydrogen bonding is well known for aroyl or acoyl substituted organic

Table 2. The intramolecular and intermolecular hydrogen bond interactions in **3a** and **3d**.

H-bonding	X	H	Y	d(X–H) (Å)	d(H–Y) (Å)	d(X–Y) (Å)	<(XHY) (°)
3a							
Intramolecular	N1	H1a	O	0.860	1.929	2.646	139.87
Intermolecular	N2	H2a	S	0.860	2.817	3.636	159.22
Intermolecular	C24	H24	S	0.930	2.689	3.376	131.36
3d							
Intramolecular	N1	H1a	O	0.860	1.595	2.657	137.49
Intermolecular	N2	H2a	S	0.860	2.710	3.540	162.80

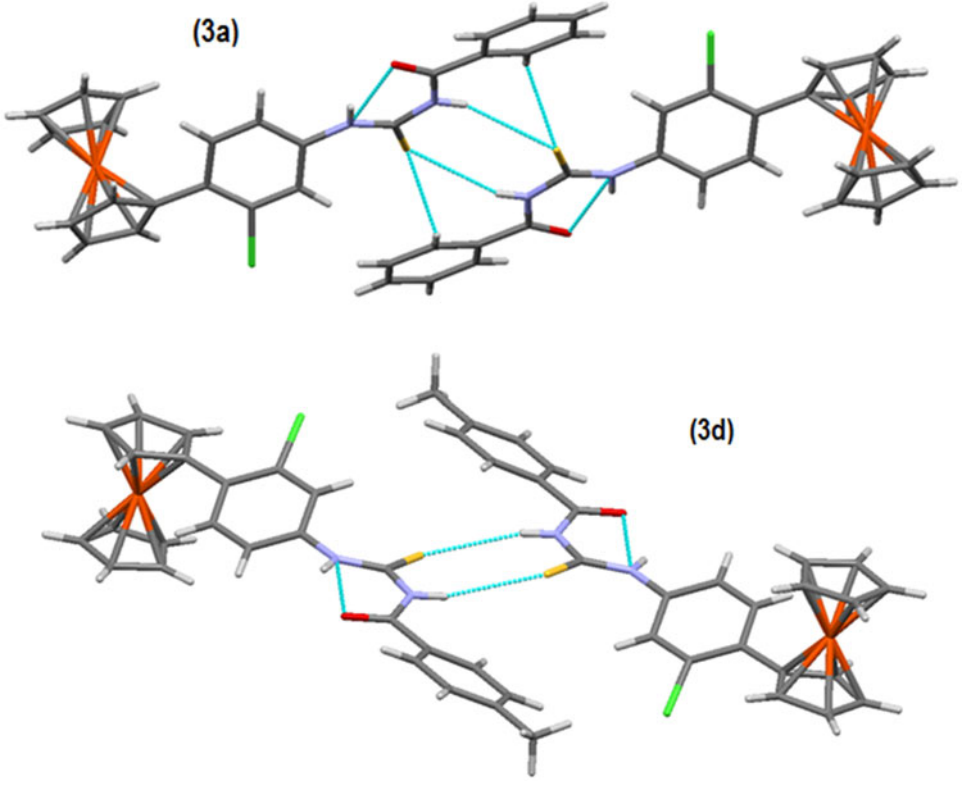

Figure 7. Dimeric structures of **3a** and **3d** mediated by hydrogen bonding interactions.

thioureas as we found in the ferrocene analogs [39–41]. This planarity normally spread the π-electronic cloud over the conjugated system and compels rings A–D to be on a sole surface, as reported for similar compounds [41, 42]. The presence of chloride on ring B destroys the co-planarity of all the rings as indicated by the inter planar angles. The inter planar angles between the planes in **3a** and **3d** are A/B = 32.49°, 29.84°; A/C = 7.07°, 5.59°; A/D = 7.21°, 16.35°; B/C = 25.46°, 27.38°; B/D = 38.87°, 45.6° and C/D = 13.94°, 18.31°, respectively. In **3d**, the presence of methyl group (electron donor) also disturbs the unidirectional charge flow and increases the inter planar angle between rings C and D in comparison to that in **3a**. However, the bond distances between A and B rings 1.482(5) (for **3a**), (C10–C11 = 1.474(3) (for **3d**), are less than the normal C–C single bond distance 1.54 Å), indicating double bond character due to resonance over these rings.

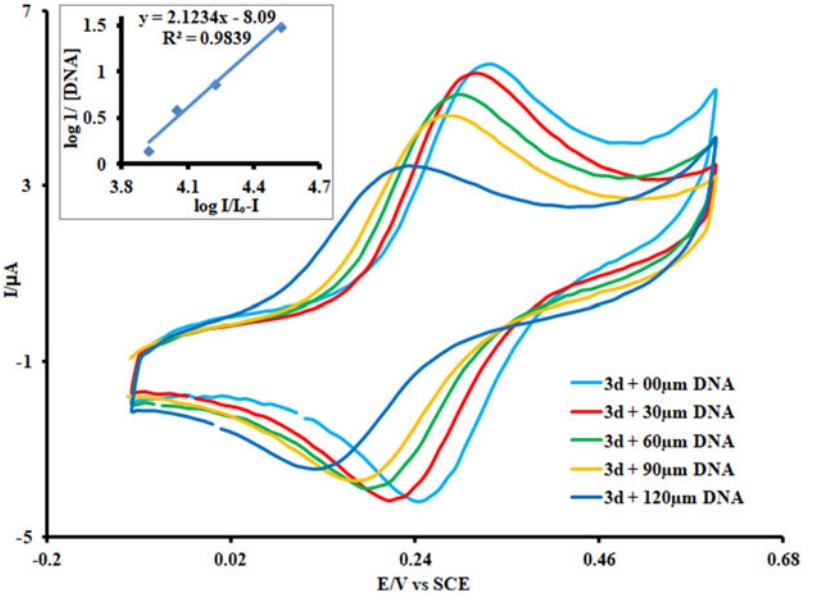

Figure 8. Cyclic voltammograms of 2 mM **3d** at 150 mVs^{-1} scan rate in the absence and presence of 30–120 µM DNA, obtained on a three electrode system: platinum disc working electrode, secondary calomel as reference electrode and platinum wire counter electrode. (Inset) Plot of log (I/I_o-I) *vs.* log (1/[DNA]) for determination of binding constant.

The two independent molecules exist in an asymmetric unit which is connected alternately to each other by the intermolecular hydrogen bonding of type NH—S, CH—O and secondary non-covalent interactions (CH—S) to produce a dimeric structure as shown in Figure 7. These intermolecular non-bonding secondary interactions are important for different properties [34, 43]. Literature studies demonstrate that compounds with stronger nonbonding interactions have more ability to bind with biological macromolecules like proteins and DNA [34, 43]. Thus, we expect good biological activity and binding of these compounds with DNA.

2.6. DNA binding studies using cyclic voltammetry

The cyclic voltammograms of **3a–3d** were utilized for probing reaction between DNA and **3a–3d**. Sample solutions in DMSO were prepared by fixing concentrations of test compounds and varying concentrations of DNA. The freshly prepared solutions were deaerated and placed for equilibration. These solutions were scanned for electrochemical response under the same conditions as discussed in the previous section (solution phase characterization by cyclic voltammetry). The cyclic voltammetry response thus obtained is useful to elaborate the reaction between the test compounds and DNA. For **3d** (a representative example), the voltammogram obtained is presented in Figure 8; there is decrease in the peak current values upon the addition of DNA to solution of **3d**. There is about 40% decrease in the peak current after the addition of 120 µM DNA, suggesting formation of an adduct of **3d** with DNA, which lowers the mobility of **3d** molecules and hence cause the decrease in current [25]. The peak potentials

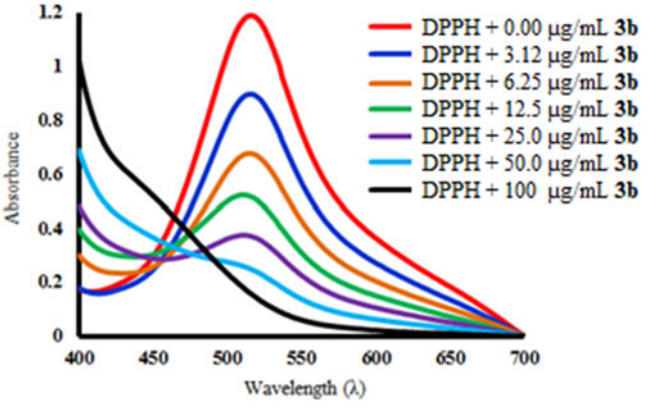

Figure 9. Variation in absorbance of DPPH spectrum with the increase in concentration of **3b** in 165 µM DPPH solution in ethanol.

also change and shift to lower values; lowering of redox potentials indicate that DNA facilitates the redox process of **3d** by providing electronic charge density from its phosphate backbone [22]. This provides evidence for electrostatic mode of interaction between DNA and **3d** [41]. Hence, the mode of interaction of **3d** with DNA was electrostatic as one can see cathodic shift and decrease in peak current on addition of increasing concentrations of DNA [20].

Figure 8 further shows that continuous addition of DNA to the solution of **3d** changes the electrochemical behavior of **3d** on the surface of the working electrode. This change in electrochemical profile has been quantified in terms of binding constant (K) and diffusion coefficient of **3d** on electrode surface. The values of binding constants (K) were calculated by the following equation [44]:

$$\text{Log } (1/[\text{DNA}]) = \log K + \log (I/I_o - I) \quad (2)$$

where I_o is the peak current of free **3d** and I is the peak current of **3d**-DNA adduct. The obtained value of binding constant was utilized to calculate the change in Gibb's free energy (ΔG) of the reaction between **3d** and DNA [44], according to the equation ($\Delta G = -RT \ln K$), and the calculated value is reported in Table 1 along with other data. The moderate value of ΔG signifies spontaneity of the **3d**-DNA interaction. The diffusion coefficients (D_o) of free compounds and compound-DNA adducts were calculated from Randles-Sevcik Equation (3) [25],

$$I_{pa} = 2.69 \times 10^5 n^{3/2} A C_o^* D_o^{1/2} \upsilon^{1/2} \quad (3)$$

where I_{pa} is the anodic peak current in amperes, v is the scan rate in V s^{-1}, C_o^* is the concentration in mol cm^{-3}, A is the cross-sectional area of electrode in cm^2 and n is the number of electrons involved in the reaction. The compound-DNA adduct formation can be justified as free molecules (with low molecular weight) easily diffuse and show more peak current, whereas when interacting with DNA, the quantity of free molecules became less, as a result decrease in current was observed and hence the lower value of D_o. The other compounds **3a–3c** responded similarly when studied for DNA interaction. Their interaction results and data obtained are reported in Table 1 and also compared with similar examples from the literature. The electrostatic mode

of interaction is the same for all screened compounds. The mechanism of interaction with DNA can be suggested as the involvement of Fe^{+2} which may bind with the DNA, followed by oxidation; the other possibility is Fe^{+2} first oxidizes to Fe^{+3} and this oxidized form then interacts with the negatively charged phosphate of the DNA helix structure, in accord with literature reports [8, 41].

2.7. Free radical scavenging screening

The DPPH method was utilized to estimate the free radical scavenging (antioxidant) potentials of **3a–3d** in ethanol [45]. Figure 9 presents the spectral profile of DPPH in the presence of **3b**. The reason behind this is free DPPH molecules are scavenged by **3b** molecules, decreasing concentration of DPPH decreasing absorbance. The decrease in absorbance at 519 nm was used to estimate the percent inhibition of the test compound by using the procedure given in Section 4. The percent inhibitions were utilized to calculate the IC_{50} value; all the compounds have similar spectral profiles of DPPH with different values for percent inhibition and hence the IC_{50} values. IC_{50} values for **3a**, **3b**, **3c** and **3d** are 25.27 μg/mL, 10.17 μg/mL, 28.02 μg/mL and 17.90 μg/mL, respectively.

Biological disorders, cancers and other diseases are associated with higher levels of reactive oxidant (RO) species (free radicals) in the body [46, 47]. Under normal physiological conditions these free radicals are tightly controlled by biological antioxidants. When biological antioxidants fail, these harmful free radicals increase in concentration, and, on increasing, these radicals injure cells by damaging lipids, proteins, DNA and sugars and initiate many degenerative diseases like cancer. Compounds **3a–3d** showed significant free radical scavenging behavior. The suggested mechanism of scavenging DPPH free radical may be donation of hydrogen from the compound to the DPPH free radical, so DPPH is no longer a free radical [48]. ^{1}H NMR values for –CSN***H*** and –CON***H*** are very downfield, which showed that these protons are labile and acidic and can easily be liberated. It is plausible that these protons are responsible for the free radical scavenging activity.

3. Conclusion

Four newly synthesized ferrocene incorporated N,N′-disubstituted thioureas (**3a–3d**) have been prepared and characterized. Compounds **3a** and **3d** were characterized by X-ray crystallography. In the solid state, these compounds have good nonbonding (van der Waals and hydrogen bonding) interactions. These compounds have significant DNA binding and free radical scavenging activity. All the synthesized compounds exhibited electrostatic mode of interaction with DNA and it is assumed that the Fe^{2+}/Fe^{3+} interacts with phosphates of double helical structure. DFT calculations were performed for the molecular structures of these compounds. The calculated electrochemical band gaps were in good correlation with experimental results of Fe^{2+}/Fe^{3+} redox reaction on the electrode surface. The lower IC_{50} values of these compounds suggest their potential as a new class of metal-based antioxidants.

4. Experimental

4.1. Materials and methods

Ferrocene, 3-chloro-4-nitroaniline, potassium thiocyanate, sodium nitrite, benzoyl chloride, 2-methylbenzoyl chloride, 3-methylbenzoyl chloride, 4-methylbenzoyl chloride, tetrabutylammonium perchlorate (TBAP), hydrochloric acid and 2,2-diphenyl-1-picrylhydrazyl (DPPH) were purchased from Sigma Aldrich (St. Louis, MO. USA) and used as received. Solvents such as ethanol, methanol, acetone, diethyl ether and petroleum ether were purified by using standard procedures [49]. Sodium salt of DNA (purchased from Acros, Geel – Belgium) was used as received. Ten millimolar stock solution of DNA was prepared in 20% aqueous DMSO. The system was buffered at pH 7 by phosphate buffer (0.1 M NaH_2PO_4 + 0.1 M NaOH) to avoid the decomposition of ferrocenium in a basic solution and protonation of the ferrocenyl group in strongly acidic conditions. Tetrabutylammoniumperchlorate (TBAP) (Fluka - Shanghai, China, 99% purity) was further purified by re-crystallization using methanol. The nucleotide to protein (N/P) ratio of 1.85 was obtained from the ratio of absorbance at 260 and 280 nm (A260/A280 = 1.85), evidenced for protein-free DNA [34]. All other reagents were of analytical grade. Doubly distilled water and absolute ethanol were used for all sample solutions. The molar absorption coefficient for DNA has been used as 6600 $M^{-1}cm^{-1}$.

^1H and ^{13}C NMR spectra were obtained using a BRUKER AVANCE 300 MHz NMR spectrometer with deuterated solvents and tetramethylsilane as an internal reference. Chemical shift values are given in ppm, coupling constants in Hz. FTIR spectra were recorded with a Thermo Scientific Nicolet-6700 FTIR spectrometer (400–4000 cm^{-1}). X-ray measurements were collected on a Bruker kappa APEXII CCD diffractometer equipped with graphite-monochromated Mo-Kα radiation ($\lambda = 0.71073$ Å) source. Cyclic voltammetry measurements were performed using an Eco Chemie Auto lab PGSTAT 12 potentiostat/galvanostat (Utrecht, The Netherlands) with the electrochemical software package GPES 4.9. A Pharma Spac UV-1800 UV-Visible Spectrophotometer (SHIMADZU, Kyoto, Japan) was used to record UV-visible spectral measurements.

4.2. Synthesis of 1-benzoyl-3-(4-ferrocenyl-3-chlorophenyl) thiourea (3a)

To solution of benzoyl chloride (0.41 mL, 3.6 mmol) in dried acetone (100 mL), potassium thiocyanate (0.35 g, 3.6 mmol) was added under N_2. 3-Chloro-4-ferrocenylaniline (1.125 g, 3.6 mmol) was added to the resulting reaction mixture and kept stirring for 4 h. The reaction mixture was then poured into ice cooled water and stirred vigorously. The solid product was filtered off and washed with deionized water. **3a** was dried in air and re-crystallized from ethyl acetate. Yield (1.3 g, 76%), Elemental analysis Cal. (%) for $C_{24}H_{19}FeN_2OSCl$: C, 60.71; H, 4.03; N, 5.90; S, 6.75. Found (%): C, 60.68; H, 4.09; N, 5.87; S, 6.72. FTIR (υ cm^{-1}): Fe-cp (481 cm^{-1}), NH (3422 cm^{-1}), C = O (1661 cm^{-1}), C = S (1137–1256 cm^{-1}), C = C Ar (1455–1592 cm^{-1}), sp^2 CH (3029.5 cm^{-1}). ^1H NMR (300 MHz, DMSO-d_6): δ 12.70 (s, 1 H, CSN*H*), 9.15 (s, 1 H, CON*H*), 7.91–7.65 (m, 7 H, C_6H_3-C_6H_5), 4.78 (s, 2 H, C_5H_4), 4.38 (s, 2 H, C_5H_4), 4.17 (s, 5 H, C_5H_5) ppm. ^{13}C NMR (75 MHz, DMSO-d_6): δ 177.91, 167.04, 135.98, 135.88, 133.93, 132.20, 131.47, 131.30, 129.31, 127.55, 125.22, 121.80, 83.47, 69.73, 68.73, 67.94 ppm.

4.3. 1-(2-Methylbenzoyl)-3-(3-chloro-4-ferrocenylphenyl) thiourea (3 b)

Compound **3b** was prepared using the same method as for **3a** except using 2-methylbenzoyl chloride in place of benzoyl chloride in equimolar ratio. Yield (1.27 g, 72%), Elemental analysis Cal. (%) for $C_{25}H_{21}FeN_2OSCl$: C, 61.43; H, 4.33; N, 5.73; S, 6.56. Found (%): C, 61.40; H, 4.29; N, 5.75; S, 6.59. FTIR (υ cm^{-1}): Fe-cp (486 cm^{-1}), NH (3403 cm^{-1}), C = O (1673 cm^{-1}), C = S (1106–1165 cm^{-1}), C = C Ar (1519–1574 cm^{-1}), sp^3 CH (3032 cm^{-1}), sp^2 CH (3159 cm^{-1}). ^{1}H NMR (300 MHz, DMSO-d_6): δ 12.59 (s, 1 H, CSN*H*), 8.84 (s, 1 H, CON*H*), 7.57 (m, 7 H, C_6H_4-C_6H_3), 4.77 (s, 2 H, C_5H_4), 4.38 (s, 2 H, C_5H_4), 4.18 (s, 5 H, C_5H_5), 2.58 (s, 3 H, CH_3) ppm. ^{13}C NMR (75 MHz, DMSO-d_6): δ 178.01, 169.57, 137.83, 135.93, 135.87, 132.57, 132.28, 132.19, 132.03, 131.29, 127.01, 126.39, 125.22, 121.81, 83.52, 69.79, 68.78, 68.23, 20.23 ppm.

4.4. 1-(3-Methylbenzoyl)-3-(3-chloro-4-ferrocenylphenyl) thiourea (3c)

Compound **3c** was prepared using the same method as for **3a** except using 3-methylbenzoyl chloride in place of benzoyl chloride in equimolar ratio. Yield (1.28 g, 73%), Elemental analysis Cal. (%) for $C_{25}H_{21}FeN_2OSCl$: C, 61.43; H, 4.33; N, 5.73; S, 6.56. Found (%): C, 61.44; H, 4.36; N, 5.72; S, 6.53. FTIR (υ cm^{-1}): Fe-cp (485 cm^{-1}), NH (3299 cm^{-1}), C = O (1673 cm^{-1}), C = S (1139–1275 cm^{-1}), C = C Ar (1519–1566 cm^{-1}), sp^3 CH (3085 cm^{-1}), sp^2 CH (3113 cm^{-1}). ^{1}H NMR (300 MHz, DMSO-d_6): δ 12.71 (s, 1 H, CSN*H*), 9.09 (s, 1 H, CON*H*), 7.87–7.51 (m, 7 H, C_6H_4, C_6H_3), 4.78 (s, 2 H, C_5H_4), 4.38 (s, 2 H, C_5H_4), 4.18 (s, 5 H, C_5H_5), 2.48 (s, 3 H, CH_3) ppm. ^{13}C NMR (75 MHz, DMSO-d_6): δ 177.84, 167.26, 139.40, 136.00, 135.86, 134.74, 132.19, 131.28, 129.19, 128.88, 128.10, 125.39, 125.23, 124.64, 121.81, 83.68, 69.86, 68.87, 21.41 ppm.

4.5. 1-(4-Methylbenzoyl)-3-(3-chloro-4-ferrocenylphenyl) thiourea (3d)

Compound **3d** was prepared using the same method as for **3a** except using 4-methylbenzoyl chloride in place of benzoyl chloride in equimolar ratio. Yield (1.35 g, 77%), Elemental analysis Cal. (%) for $C_{25}H_{21}FeN_2OSCl$: C, 61.43; H, 4.33; N, 5.73; S, 6.56. Found (%): C, 61.46; H, 4.36; N, 5.71; S, 6.54. FTIR (υ cm^{-1}): Fe-cp (479 cm^{-1}), NH (3247 cm^{-1}), C = O (1663 cm^{-1}), C = S (1032–1105 cm^{-1}), C = C Ar (1524–1568 cm^{-1}), sp^3 CH (3019 cm^{-1}), sp^2 CH (3157 cm^{-1}). ^{1}H NMR (300 MHz, DMSO-d_6): δ 12.74 (s, 1 H, CSN*H*), 9.08 (s, 1 H, CON*H*), 7.56 (m, 7 H, C_6H_4-C_6H_3), 4.84 (s, 2 H, C_5H_4), 4.43 (s, 2 H, C_5H_4), 4.22 (s, 5 H, C_5H_5), 1.28 (s, 3 H, CH_3) ppm. ^{13}C NMR (75 MHz, DMSO-d_6): δ 166.92, 153.53, 145.10, 136.02, 135.81, 133.98, 132.20, 131.30, 130.02, 127.58, 125.22, 121.82, 83.49, 69.73, 68.71, 67.95, 21.79 ppm.

4.6. Single crystal X-ray diffraction analysis

X-ray measurements were made on a Bruker Kappa APEXII CCD diffractometer equipped with graphite-monochromated Mo-Kα radiation (λ = 0.71073 Å) source. The data collection used ω scans, and a multi-scan absorption correction was applied. The structure was solved by using a SHELXS97 (Sheldrick, 273 2008) program and it was refined by full-matrix least-squares using SHELXL-97 [50]. Different software like Mercury and ENCIFER were used to draw the structures of the analyzed compounds.

4.7. Free radical scavenging screening

The antioxidant activities of **3a–3d** were determined by using the DPPH method [48]. The sample solutions were prepared by keeping constant concentration of DPPH (165 μM) with increasing concentration of compounds (3.125, 6.25, 12.5, 25, 50, 100 μg mL^{-1}) in ethanol and buffered at pH 6 (0.1 M NaH_2PO_4 + 0.1 M NaOH). All these mixture were kept in the dark for 30 min and absorbance was measured at 517 nm in dim light using a Shimadzu 1800 UV-Vis spectrophotometer. From the mean value of three readings, % inhibition was calculated by using the equation [% inhibition = 100 (1 – A_s/A_o)], where A_o and A_s are the absorbance of DPPH solution (at 517 nm) in the absence and presence of test samples, respectively [45, 48].

Disclosure statement

No potential conflict of interest was reported by the authors.

Funding

The authors are thankful to the Higher Education Commission (HEC) Pakistan and Pakistan Academy of Science (PAS), Islamabad, Pakistan, for their financial support.

References

[1] T. Boulikas, M. Vougiouka. *Oncol. Rep.*, **10**, 1663 (2003).
[2] A.-M. Florea, D. Büsselberg. *Cancers. (Basel)*, **3**, 1351 (2011).
[3] J. Reedijk. *Proc. Natl. Acad. Sci. USA.*, **100**, 3611 (2003).
[4] C.G. Hartinger, P.J. Dyson. *Chem. Soc. Rev.*, **38**, 391 (2009).
[5] K. Wu, S. Liu, Q. Luo, W. Hu, X. Li, F. Wang, R. Zheng, J. Cui, P.J. Sadler, J. Xiang, Q. Shi, S. Xiong. *Inorg. Chem.*, **52**, 11332 (2013).
[6] F. Giannini, G. Süss-Fink, J. Furrer. *Inorg. Chem.*, **50**, 10552 (2011).
[7] G. Gasser, I. Ott, N. Metzler-Nolte. *J. Med. Chem.*, **54**, 3 (2011).
[8] D.R. Van Staveren, N. Metzler-Nolte. *Chem. Rev.*, **104**, 5931 (2004).
[9] C. Ornelas. *New J. Chem.*, **35**, 1973 (2011).
[10] M. Jamil, M. Zubair, A.A. Altaf, M.A. Farid, M.T. Hussain, N. Rasool, I.H. Bukhari, V.U. Ahmad. *J. Chem. Soc. Pakistan*, **35**, 737 (2013).
[11] M. Jamil, M. Zubair, M.A. Farid, A.A. Altaf, N. Rasool, I.H. Bukhari, K. Rizwan, V.U. Ahmad. *J. Chem. Soc. Pakistan*, **35**, 834 (2013).
[12] M. Jamil, M. Zubair, N. Rasool, A.A. Altaf, K. Rizwan, S. Hafeez, I.H. Bukhari, P. Langer. *Asian J. Chem.*, **25**, 5328 (2013).
[13] M. Jamil, M. Zubair, M.A. Farid, A.A. Altaf, N. Rasool, F.-U.-H. Nasim, M. Ashraf, M.A. Rashid, S.A. Ejaz, A. Yaqoob, V.U. Ahmad. *J. Chem. Soc. Pakistan*, **36**, 491 (2014).
[14] A. Shakeel, A.A. Altaf, A.M. Qureshi, A. Badshah. *J. Drug Des. Med. Chem.*, **2**, 10 (2016).
[15] S.H. van Rijt, P.J. Sadler. *Drug Discov. Today.*, **14**, 1089 (2009).
[16] M.F. Fouda, M.M. Abd-Elzaher, R.A. Abdelsamaia, A.A. Labib. *Appl. Organometal. Chem.*, **21**, 613 (2007).
[17] H. Tamura, M. Miwa. *Chem. Lett.*, **26**, 1177 (1997).
[18] D. Osella, M. Ferrali, P. Zanello, F. Laschi, M. Fontani, C. Nervi, G. Cavigiolio. *Inorg. Chim. Acta*, **306**, 42 (2000).
[19] B. Lal, A. Badshah, A.A. Altaf, M.N. Tahir, S. Ullah, F. Huq. *Aust. J. Chem.*, **66**, 1352 (2013).

[20] S. Hussain, A. Badshah, B. Lal, R.A. Hussain, S. Ali, M.N. Tahir, A.A. Altaf. *J. Coord. Chem.*, **67**, 2148 (2014).
[21] M. Ayaz, A. Badshah, B. Lal, A.A. Altaf, S. Kamal, S. Ali, I. Ud-Din, A. Shah. *J. Chem. Soc. Pakistan*, **37**, 974 (2015).
[22] B. Lal, S. Akhter, A.A. Altaf, A. Badshah, R.A. Hussain, H. Li. *Int. J. Electrochem. Sci.*, **11**, 1632 (2016).
[23] M. Marcaccio, F. Paolucci, C. Paradisi, S. Roffia, C. Fontanesi, L.J. Yellowlees, S. Serroni, S. Campagna, G. Denti, V. Balzani. *J. Am. Chem. Soc.*, **121**, 10081 (1999).
[24] Š. Komorsky-Lovrić, M. Lovrić. *Anal. Chim. Acta*, **305**, 248 (1995).
[25] A.J. Bard, L.R. Faulkner, J. Leddy, C.G. Zoski. *Electrochemical Methods: Fundamentals and Applications*, Wiley, New York, NY (1980).
[26] Y. Wang, E.I. Rogers, R.G. Compton. *J. Electroanal. Chem.*, **648**, 15 (2010).
[27] C.O. Laoire, E. Plichta, M. Hendrickson, S. Mukerjee, K. Abraham. *Electrochim. Acta*, **54**, 6560 (2009).
[28] I. Noviandri, K.N. Brown, D.S. Fleming, P.T. Gulyas, P.A. Lay, A.F. Masters, L. Phillips. *J. Phys. Chem. B*, **103**, 6713 (1999).
[29] M. Marinov, S. Minchev, N. Stoyanov, G. Ivanova, M. Spassova, V. Enchev. *Croat. Chem. Acta*, **78**, 9 (2005).
[30] B.W. D'Andrade, S. Datta, S.R. Forrest, P. Djurovich, E. Polikarpov, M.E. Thompson. *Org. Electron.*, **6**, 11 (2005).
[31] A.A. Altaf, A. Shahzad, Z. Gul, S.A. Khan, A. Badshah, M.N. Tahir, Z.I. Zafar, E. Khan. *J. Chem.*, **2015**, 1 (2015).
[32] F. Asghar, S. Fatima, S. Rana, A. Badshah, I.S. Butler, M.N. Tahir. *Dalton Trans.*, **47**, 1868 (2018).
[33] S. Chandrasekar, V. Balachandran, H.-S. Evans, A. Latha. *Spectrochim. Acta A Mol. Biomol. Spectrosc.*, **143**, 136 (2015).
[34] F. Javed, A.A. Altaf, A. Badshah, M.N. Tahir, M. Siddiq, A. Shah, S. Ullah, B. Lal. *J. Coord. Chem.*, **65**, 969 (2012).
[35] A.A. Altaf, S. Kausar, M. Hamayun, B. Lal, M.N. Tahir, A. Badshah. *J. Mol. Struct.*, **1146**, 130 (2017).
[36] A.A. Altaf, M. Hamayun, B. Lal, M.N. Tahir, A.A. Holder, A. Badshah, D.C. Crans. *Dalton Trans.*, **47**, 11769 (2018).
[37] I. Koca, A. Özgür, K.A. Coşkun, Y. Tutar. *Bioorg. Med. Chem.*, **21**, 3859 (2013).
[38] S. Saeed, N. Rashid, P.G. Jones, M. Ali, R. Hussain. *Eur. J. Med. Chem.*, **45**, 1323 (2010).
[39] J. Haribabu, G.R. Subhashree, S. Saranya, K. Gomathi, R. Karvembu, D. Gayathri. *J. Mol. Struct.*, **1094**, 281 (2015).
[40] A. Saeed, S. Ashraf, J.M. White, D.B. Soria, C.A. Franca, M.F. Erben. *Spectrochim. Acta A Mol. Biomol. Spectrosc.*, **150**, 409 (2015).
[41] B. Lal, A. Badshah, A.A. Altaf, M.N. Tahir, S. Ullah, F. Huq. *Dalton Trans.*, **41**, 14643 (2012).
[42] R. Gul, A.A. Altaf, A. Badshah, A. Shah, Z.U. Rehman, R. Naz, M.N. Tahir, A. Junaid. *Med. Chem.*, **12**, 684 (2016).
[43] K.E. Riley, K.-A. Tran. *Crystals*, **7**, 273 (2017).
[44] A. Shah, M. Zaheer, R. Qureshi, Z. Akhter, M.F. Nazar. *Spectrochim. Acta A Mol. Biomol. Spectrosc.*, **75**, 1082 (2010).
[45] A.A. Altaf, A. Badshah, B. Lal, S. Murtaza, P.B. Chatterjee, K. Akbar, D.C. Crans. *Appl. Organometal. Chem.*, **32**, e4334 (2018).
[46] D.B. Zorov, M. Juhaszova, S.J. Sollott. *Physiol. Rev.*, **94**, 909 (2014).
[47] X. Wen, J. Wu, F. Wang, B. Liu, C. Huang, Y. Wei. *Free Radic. Biol. Med.*, **65**, 402 (2013).
[48] K. Pyrzynska, A. Pękal. *Anal. Methods*, **5**, 4288 (2013).
[49] A.B. Pangborn, M.A. Giardello, R.H. Grubbs, R.K. Rosen, F.J. Timmers. *Organometallics*, **15**, 1518 (1996).
[50] G.M. Sheldrick. *Acta Crystallogr. A*, **64**, 112 (2008).